Author Manuscript

Author Manuscript

Author Manuscript

Author Manuscript

HHS Public Access

Author manuscript

Free Radic Biol Med. Author manuscript; available in PMC 2020 December 22.

Published in final edited form as:

Free Radic Biol Med. ; 147: 167–174. doi:10.1016/j.freeradbiomed.2019.12.020.

Increased formation of reactive oxygen species during tumor growth: *Ex vivo* low-temperature EPR and *in vivo* bioluminescence analyses

Gang Cheng[1,2], **Jing Pan**[3], **Radoslaw Podsiadly**[8], **Jacek Zielonka**[1,2,4], **Alexander M. Garces**[9,10], **Luiz Gabriel Dias Duarte Machado**[9,11], **Brian Bennett**[9], **Donna McAllister**[5], **Michael B. Dwinell**[4,5,6], **Ming You**[3,4,7], **Balaraman Kalyanaraman**[1,2,4,7]

[1]Department of Biophysics, Medical College of Wisconsin, 8701 Watertown Plank Road, Milwaukee, WI 53226, United States [2]Free Radical Research Center, Medical College of Wisconsin, 8701 Watertown Plank Road, Milwaukee, WI 53226, United States [3]Pharmacology and Toxicology, Medical College of Wisconsin, 8701 Watertown Plank Road, Milwaukee, WI 53226, United States [4]Cancer Center, Medical College of Wisconsin, 8701 Watertown Plank Road, Milwaukee, WI 53226, United States [5]Department of Microbiology & Immunology, Medical College of Wisconsin, 8701 Watertown Plank Road, Milwaukee, WI 53226, United States [6]Department of Surgery, Medical College of Wisconsin, 8701 Watertown Plank Road, Milwaukee, WI 53226, United States [7]Center for Disease Prevention Research, Medical College of Wisconsin, 8701 Watertown Plank Road, Milwaukee, WI 53226, United States [8]Institute of Polymer and Dye Technology, Faculty of Chemistry, Lodz University of Technology, Stefanowskiego 12/16, 90-924 Lodz, Poland [9]Department of Physics, Marquette University, 1420 West Clybourn Street, Milwaukee, WI 53233, United States [10]Present address: Department of Biophysics, Medical College of Wisconsin, 8701 Watertown Plank Road, Milwaukee, WI 53226, United States [11]Present address: Faculty of Medicine, Sapienza Università di Roma, Piazzale Aldo Moro 5, 00185-Roma, Rome, Italy

Abstract

Previous studies have shown that reactive oxygen species (ROS) such as superoxide or hydrogen peroxide generated at low levels can exert a tumor-promoting role *via* a redox-signaling mechanism. Reports also suggest that both tumorigenesis and tumor growth are associated with enhanced ROS formation. However, whether ROS levels or ROS-derived oxidative marker levels increase during tumor growth remains unknown. In this study, *in vivo* bioluminescence imaging with a boronate-based pro-luciferin probe was used to assess ROS formation. Additionally, probe-free cryogenic electron paramagnetic resonance was used to quantify a characteristic aconitase $[3Fe4S]^{+}$ center that arises in the tumor tissue of mouse xenografts from the reaction of the native $[4Fe4S]^{2+}$ cluster with superoxide. Results indicated that tumor growth is accompanied by increased ROS formation, and revealed differences in oxidant formation in the inner and outer

Publisher's Disclaimer: This is a PDF file of an unedited manuscript that has been accepted for publication. As a service to our customers we are providing this early version of the manuscript. The manuscript will undergo copyediting, typesetting, and review of the resulting proof before it is published in its final form. Please note that during the production process errors may be discovered which could affect the content, and all legal disclaimers that apply to the journal pertain.

Author Manuscript Author Manuscript Author Manuscript Author Manuscript

sections of tumor tissue, respectively, demonstrating redox heterogeneity. Studies using luciferin and pro-luciferin probes enabled the assessment of tumor size, ROS formation, and bioenergetic status (*e.g.*, ATP) in luciferase-transfected mice tumor xenografts. Probe-free *ex vivo* low-temperature electron paramagnetic resonance can also be translated to clinical studies.

Graphical Abstract

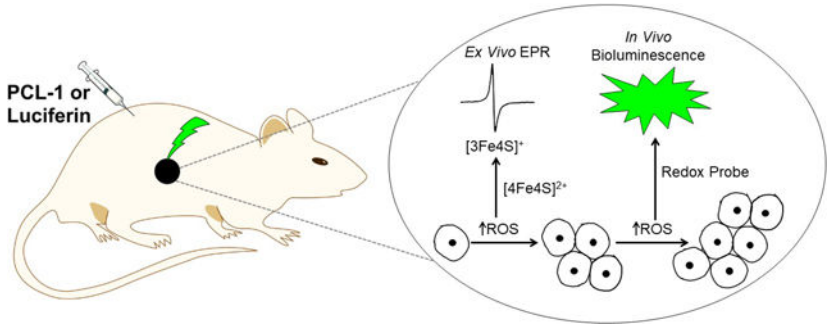

Keywords

EPR; mitochondria; tumor growth; oxidants; bioluminescence

Introduction

Emerging evidence suggests that reactive oxygen species (ROS) (*e.g.*, superoxide and hydrogen peroxide [H_2O_2]) generated at low levels in the mitochondria exert a tumor-promoting role via a redox-signaling mechanism [1–5]. This is contrary to conventional thinking that suggests ROS always induce cytotoxic effects in normal and cancer cells. ROS play a dual role, causing oncogenic mutations and/or activating oncogenic pathways [6]. Antioxidants could, therefore, suppress tumor initiation or progression and metastasis in some cancers [7]. The success of conventional cytotoxic antitumor and radiation therapies is dependent on the damaging effects of ROS in tumors. Thus, depending on the type and maturity of the tumor, the biological and metabolic environment, and the level of ROS activity, ROS may exert either tumor-promoting or tumor-inhibiting effects [8]. In tumor models, antioxidant supplementation has also yielded paradoxical effects [9, 10]. In lung cancer and melanoma mouse models, antioxidant supplementation enhanced tumor progression and metastasis [9, 10]. Dietary supplementation with antioxidants also increased prostate cancer incidence in humans [11]. However, the longitudinal measurements of ROS levels during tumor growth and tumor progression have not been previously carried out.

EPR spectroscopy detects unpaired electrons, including those in free radicals and in many redox states of transition metal ions (*e.g.*, Fe^{III}, Cu^{II}, $Mn^{II/III/IV}$) and in metal clusters (*e.g.*, $[2Fe2S]^{+}$, $[3Fe4S]^{0/+}$, $[4Fe4S]^{+}$). EPR is often diagnostic for individual paramagnetic species, and typically 12–16 of the approximately 20 signals expected from mitochondria can be assigned depending on the tissue and redox status [12]. EPR is also quantitative, and the amounts of species in the paramagnetic state can be estimated by computer fitting. EPR detection of mitochondrial redox centers requires cryogenic temperatures (5–40 K). At such

Author Manuscript Author Manuscript Author Manuscript Author Manuscript

low temperatures, unpaired electrons remain free to migrate between redox centers with appreciable exchange interactions and adopt statistical distributions according to the centers' midpoint potentials. However, diffusion and active transport of molecules cease. Therefore, low-temperature EPR of flash-frozen intact tissue or cell samples provides a snapshot of the redox status of the various mitochondrial respiratory chain complexes at the time of freezing, and reports on the midpoint potentials of the individual redox centers and the integrity of their intramolecular electron transfer pathways. EPR also reports on oxidative stress history. Interrogation of the ROS-mediated (as superoxide) oxidative partial disassembly of the mitochondrial aconitase EPR-silent $[4Fe4S]^{2+}$ cluster to the characteristic EPR-active $[3Fe4S]^{+}$ center [13, 14] provides a snapshot of the ROS burden of the cell, whereas EPR-detected overexpression of catalase measures a compensatory response to chronic ROS exposure [15, 16].

In the present work, we address the knowledge gap that currently exists concerning the role of ROS in tumorigenesis by rigorously investigating the association between tumor growth over time and oxidative biomarker formation, assayed by *ex vivo* EPR in a breast cancer mouse xenograft model. EPR was used to monitor the instantaneous ROS burden, as aconitase $[3Fe4S]^{+}$; the chronic ROS burden, as catalase ferriheme; and the mitochondrial respiratory chain metabolic potential, as measured by the characteristic 'g=1.92' signal due to reduced low-potential $[2Fe2S]^{+}$ and $[4Fe4S]^{+}$ clusters [16]. We have additionally used *in vivo* bioluminescence imaging to measure oxidant formation and to assess the bioenergetic status in mice tumor xenografts. Tumor growth is typically monitored by measuring the intensity of bioluminescence signal intensity in luciferase-transfected cancer cell mice xenografts [17, 18]. The substrate, luciferin, is injected into tumor-bearing mice xenografts, and the green bioluminescence is measured as a function of tumor growth. Recently, a cell-permeable smallmolecular-weight pro-luciferin peroxy-caged luciferin probe (PCL-1) was used to noninvasively image ROS in mice [19, 20]. This approach enables monitoring of oxidants in tumor cells due to selective localization of luciferase in those cells. Because bioluminescence intensity depends not only on the nature and levels of oxidants formed but also on tumor size, the number of tumor cells, and intracellular ATP level, parallel analysis using luciferin substrate revealed information about *in vivo* bioenergetic status as well (*e.g.*, ATP) [18].

Experimental Design

Cell culture

The human breast cancer cell line MDA-MB-231, human pancreatic cancer cell line MiaPaCa-2, human lung cancer cell line H2030, and human oral cancer cell line SCC-9 were acquired from the American Type Culture Collection, where they are regularly authenticated. Cells were stored in liquid nitrogen and used within six months after thawing. MDA-MB-231 and MiaPaCa-2 cells were grown at 37°C in DMEM, 10% fetal bovine serum, penicillin (100 U/ml), and streptomycin (100 μg/ml). H2030 and SCC-9 cells were maintained in RPMI 1640 medium supplemented with 10% fetal bovine serum, penicillin (100 U/ml), and streptomycin (100 μg/ml). The MDA-MB-231-luc, MiaPaCa-2-luc, H2030-luc, and SCC-9-luc cell lines stably expressing firefly luciferase were cultured under the

Author Manuscript Author Manuscript Author Manuscript Author Manuscript

same conditions as the parental cell lines. Cells were cultured at 37°C in a humidified atmosphere of 5% CO_2 in air. All cell lines are regularly assessed for growth characteristics and tumorigenicity in nude mice.

Xenograft experiments

All small animal protocols were annually approved by the Medical College of Wisconsin Institutional Animal Care and Use Committee. Five- to eight-week-old male non-obese diabetic (NOD)/severe combined immunodeficiency disease (SCID) mice were used for these experiments. For the EPR study, MDA-MB-231 cells (1×10^6 cells in 200 μl of a mixture of 1:1 PBS/Matrigel) were injected into the right mammary fat pad. Two days after injecting the cells, mice were divided into five groups for EPR sample harvesting every 2 weeks till week 10. Mice were sacrificed at each experimental time point for tumor harvesting. Tumor growth was monitored by tumor weight. For the PCL-1 study, MDA-MB-231-luc cells (1×10^6 cells in 200 μl of a mixture of 1:1 PBS/Matrigel) were subcutaneously implanted on the left flank, MiaPaCa-2-luc cells (1×10^6 cells in 200 μl of a mixture of 1:1 PBS/Matrigel) were orthotopically engrafted to the pancreas, and SCC-9-luc cells (1×10^5 cells in 30 μl PBS) were injected into the lateral portion of the tongue. For tissue ATP monitoring model, H2030-luc lung cancer cells were injected through the left rib cage of mice into the left lung as an orthotopic lung cancer model. Tumor establishment and growth were monitored by injecting D-luciferin and detecting bioluminescence using the Lumina IVIS-100 In Vivo Imaging System (PerkinElmer Inc., Waltham, MA).

Ex vivo EPR and in vivo bioluminescence imaging studies in a mouse xenograft model

We used three independent protocols to noninvasively and sequentially monitor tumor size, bioenergetic status, and ROS production in mice (Fig. 1). Bioluminescence imaging (BLI) was based on the ATP-dependent, firefly luciferase-catalyzed oxidation of luciferin accompanied by light emission. The experimental design for *in vivo* imaging of tumor growth and ROS, and for *ex vivo* monitoring of redox status markers and oxidative biomarkers in tumor tissues is summarized in Fig. 1. To monitor tumor size, mice were injected with luciferin. The bioluminescence signal was proportional to the number of cancer cells expressing luciferase (Fig. 1, *tumor size imaging*). Because the reaction also required ATP, the same reaction was used to monitor changes in ATP level when tumor size was not a variable. Therefore, mice imaged for tumor size were imaged the following day for ATP, 1 h after administering the drug that is being tested. To detect ROS, PCL-1 was used, which upon oxidation yielded luciferin *in situ* that was further oxidized in luciferin-transfected tumor cells producing luminescence (Fig. 1, *ROS imaging*) [19, 20]. Luciferin and PCL-1 are cleared within hours, so they can be used sequentially after 24 h [19, 20].

Low-temperature EPR spectroscopy

EPR was carried out using a spectrometer system [15] with features that are optimized for the study of signals from mitochondrial components in cells and tissues. The signals are weak overall and broad, and they contain a wide range of intensities and line widths. Thus, excellent field, frequency (ambient temperature), and cryogenic temperature stability over time for lengthy acquisitions is essential, and a highly sensitive resonator and a very wide dynamic range in both field and intensity are desirable. EPR signals shown herein were

Author Manuscript Author Manuscript Author Manuscript Author Manuscript

recorded at 12 K, 5 mW microwave power, and 9.49 GHz microwave frequency, and employing 10 G (1.0 mT) magnetic field modulation at 100 kHz, 1.0 G (0.1 mT) digital field resolution, and a time constant equivalent to 1.0 G (0.1 mT). Additional spectra were recorded at 40 K to deconvolute the aconitase $[3Fe4S]^{+}$ signal from the S3 $[3Fe4S]^{+}$ signal from Complex II [12]. Relative intensities of isolated signals were determined by simple measurement of peak-to-trough intensities and the absolute concentrations of species were determined by single or double integration of representative spectra, which were calibrated by comparison with integrations of simulated spectra and referenced to a standard. Overlapping signals were quantified by fitting to a library of computed spectra as in earlier work [12].

Harvesting of tissues for low-temperature EPR

Sample harvesting procedures for both muscle and soft tissue were developed to ensure that the low-temperature signals from *ex vivo* samples reflected the functional mitochondrial respiratory chain. The two key criteria for reproducible and artifact-free EPR are that tissue must be rapidly harvested and deep-frozen within 3 min of harvesting, and that tissue should never be thawed and refrozen. Animal tissue work has shown that for “large” samples (*i.e.*, 0.3 g, the ideal size for an X-band EPR sample), the optimum procedure is to (i) rapidly excise the tissue as a single piece; (ii) immediately place the issue in a syringe barrel that is connected to a ventilated EPR tube via the syringe’s standard Luer outlet (not a needle) by a short piece of silicone tubing; and (iii) extrude the tissue into the EPR tube, push it to the bottom with a thin plunger, and deep freeze it by plunging the filled tube into liquid nitrogen or nitrogen-cooled isopentane. For small samples (*e.g.*, <0.1 g), tissue was (i) excised, either by scalpel or biopsy punch, (ii) cut into pieces ($2\times2\times2$ mm^3), and (iii) frozen in liquid nitrogen. The frozen tissue was subsequently introduced into a nonventilated EPR tube containing 1 cm depth of frozen 50% glycerol:50% water, pushed to the bottom, and covered with another 1 cm depth of cold 50% glycerol:50% water, while simultaneously slowly being frozen in liquid nitrogen. Samples were stored at −80°C; EPR signals were observed to be completely stable at this temperature for at least six months [12].

Synthesis of PCL-1

A modification of the published synthetic protocol [19] was employed to prepare the PCL-1 probe according to the procedure shown in Figure 2 [21] using 4-(bromomethyl)benzeneboronic acid and 6-hydroxy-2-cyanobenzo-thiazole as the starting materials.

Results

Detection of oxidized aconitase as an oxidative marker using ex vivo EPR

Triple-negative breast cancer mice xenografts were used in the study. At 2, 4, 6, 8, and 10 weeks after implantation of MDA-MB-231 cells, tumors were isolated, weighed, and flash frozen in liquid nitrogen within 3 min. As shown in Fig. 3A, the tumor weight increased with time. The EPR signal of oxidized aconitase $[3Fe4S]^{+}$, at ~3400 G (340 mT; $g\approx2.02$) (indicated by the arrow in Fig. 3B, top), increased with time, reaching the maximum intensity in 8–10 weeks (Fig. 3B, 3C). The actual concentrations of oxidatively damaged

Author Manuscript Author Manuscript Author Manuscript Author Manuscript

aconitase in tumors, determined from the $[3Fe4S]^+$ signal intensities, ranged from 0.2 μM after 2 weeks to 0.8 μM after 10 weeks (Fig. 3C). This longitudinal increase in the amount of aconitase $[3Fe4S]^+$ is clear evidence for significant elevation of ROS during tumorigenesis and tumor growth [12–14, 22–24].

In another group of MDA-MB-231-luc-based mice xenografts, we monitored tumor size (tumor growth) *in vivo* by measuring luciferin-derived bioluminescence. As shown in Fig. 4, the bioluminescence signal is proportional to the number of cells expressing luciferase (*i.e.*, tumor growth).

Ex vivo EPR: Tumor heterogeneity and redox activation

An observation was made that the larger, more mature tumors exhibited a stratified histology, consisting of two distinct tissue types that varied by color and texture (Fig. 5A). EPR was therefore used to investigate whether these two types of tissue, one of which was largely present in the inner mass of the tumor while the other predominated on the outer surface, exhibited any differences in ROS biomarkers and metabolic redox potential. The relevance of such a study to cancer biology is underscored by the finding that tumor hypoxia and glycolysis are selectively increased in the inner sections of growing tumors [25]. EPR spectroscopic interrogation identified a number of redox- and ROS-related signals that, in some cases, were not clearly identified in the spectra of the holo-tumors. The signals are labeled as follows in Fig. 5B: *Cat*, ferriheme in catalase; *Tf*, Fe(III) in transferrin; *H-a*, heme *a* from Complex IV; *N3* and *N4b*, g_3 resonances from the low-potential N3 and N4 iron-sulfur clusters of Complex I; *Acn*, aconitase $[3Fe4S]^+$; and *FeS*, a composite signal due to g_2 or $g\perp$ resonances from Complex I (N1b, N2, N3, N4) and Complex II (S1, S2) reduced $[2Fe2S]^+$ and $[4Fe4S]^+$ signals. Comparison of the EPR spectra from the two distinct tissue types indicated significant differences in the intensities of *Cat, Tf, H-a, Acn, FeS, N4b*, and the lowest-potential complex I FeS cluster, N3 (*N3*). While the outer tumor tissue did exhibit signs of oxidative stress similar to those observed in the holo-tumor (an elevated *Acn* signal compared with those from younger samples, and a small but detectable *Cat* signal), the spectrum of the inner tissue exhibited a further twofold increase in *Acn* and a strong increase in the *Cat* signal. The increase in the catalase expression could be attributed to a compensatory response to enhanced ROS formation in the hypoxic core of the tumor tissue [25]. The large *FeS* signal and detectable *N3* signal from the outer tumor tissue indicated a normal (*i.e.*, low) redox potential; the N3 midpoint potential is close to that of the NADH/NAD couple that governs the redox status in healthy tissue and its presence suggests a functional mitochondrial respiratory chain. In contrast, the inner tumor tissue spectrum indicated (i) extinction of the *N3* signal, (ii) fourfold diminution of the *FeS* signal, and (iii) a well-defined *H-a* signal. Each of these observations indicates an elevated mitochondrial redox potential and, therefore, a diminished thermodynamic driving force for oxidative phosphorylation, consistent with the reported increased reliance on glycolysis. An increased signal intensity of transferrin is typically observed under oxidative stress conditions [26–28]. The observation of a two- to threefold larger *Tf* signal in inner tissue compared to outer tissue is consistent with the finding that hypoxic preconditioning increased transferrin-bound iron in cells [29].

Author Manuscript Author Manuscript Author Manuscript Author Manuscript

ROS measurements: In vivo bioluminescence imaging

Oxidants such as H_2O_2, peroxynitrite ($ONOO^-$), and hypochlorous acid (HOCl) react with the PCL-1 probe to form luciferin *in situ* that is oxidized by the luciferase in luciferase-transfected tumor cells [21, 30] (Fig. 6). PCL-1 probe administered after tumor implantation will give a snapshot of oxidants generated during tumor growth.

Ex vivo EPR measurements showed that formation of oxidized aconitase was maximal in tumor tissue isolated after 8–10 weeks (Fig. 3). Therefore, we used mice xenografts bearing MDA-MB-231-luc tumors implanted for 10 weeks for *in vivo* ROS detection using bioluminescence imaging. Injection of luciferin into mice-bearing breast tumor expressing luciferase led to a rapid increase in bioluminescence in 10 min, followed by a steep decrease. On the other hand, injection of the same dose of PCL-1 probe led to slower but more persistent buildup of the bioluminescence signal, consistent with a slow release of luciferin upon oxidation of the PCL-1 probe by endogenous H_2O_2 (Fig. 7). These findings suggest that comparing the time course of bioluminescence from both luciferin and PCL-1 should yield important information on *in vivo* ROS formation in mice xenografts. Because ROS-independent factors controlling the degree of PCL-1-derived luminescence also affect luciferin bioluminescence (due to their structural similarities), we normalized the BLI signal from PCL-1 to the signal from the luciferin injection (the day after the PCL-1 experiment) to account for ROS-independent factors controlling BLI signal intensity.

In vivo BLI also was used to monitor tumor growth and ROS formation in luciferase-expressing human oral cancer SCC-9 xenografts in NOD/SCID mice (Figs. S1 and S2). To monitor tumor size, mice were injected with luciferin. As show in Fig. S2, there was a rapid increase in bioluminescence the cleared almost completely within 1 h (red trace). Conversely, administration of the same dose of the PCL-1 probe led to a slower but persistent buildup of the bioluminescence signal (Fig. S2, blue trace). This is attributed to a slow, oxidant-indicated release of luciferin from PLC-1. Similar results were obtained in pancreatic cancer xenograft model (Fig. S3), demonstrating the applicability of this approach to different *in vivo* tumor models, as long as the cells of interest express luciferase.

Bioluminescence imaging: In vivo bioenergetics

The bioluminescence signal generation during oxidation of luciferin by luciferase requires the presence of ATP as a cosubstrate. Therefore, we envisioned that bioluminescence measurements could be used to monitor the effects of drugs and other agents on the bioenergetic status of tumor cells in live animals. As a proof of principle, we used lung-tumor-bearing mice to show the feasibility of monitoring adenosine triphosphate (ATP) in tumor cells *in vivo*. Two major pathways of ATP generation include glycolysis and mitochondrial respiration. Mitochondria use oxidative phosphorylation (OXPHOS) to generate ATP. Drugs and compounds (*e.g.*, honokiol) inhibiting OXPHOS decrease ATP generation (Fig. 8). Briefly, tumors were allowed to grow for 30 days; on day 31, mice were examined by magnetic resonance imaging (MRI) to determine tumor size (Fig. 8C), and by BLI for the basal signal intensity (before treatment) (Fig. 8B). On day 32, mice were given honokiol and the ATP level was markedly decreased as measured by BLI 1 h later (Fig. 8B). On day 33, mice were imaged again by MRI to confirm there was no change in tumor size

Author Manuscript Author Manuscript Author Manuscript Author Manuscript

(Fig. 8), and bioluminescence intensity was measured to determine if the ATP level recovered (Fig. 8). These data demonstrate the feasibility of monitoring the temporal depletion of ATP in tumors *in vivo* upon administration of OXPHOS inhibitors.

Discussion

In this work, we address the long-standing question concerning ROS generation and tumor growth or tumorigenesis. Cryogenic-temperature *ex vivo* EPR spectroscopy provided evidence that tumorigenesis and tumor maturation are accompanied by an increase in oxidant formation. These results were supported by *in vivo* bioluminescence determinations of ROS formation in tumors. Additionally, EPR revealed significant differences in the oxidant burdens and redox-dependent metabolic potentials between the inner core tissue and outer tissue of tumors. These studies indicate that the inner core tissue of late-stage tumors undergoes enhanced oxidative stress, as evidenced by elevated aconitase and catalase signals, and has a diminished potential for oxidative phosphorylation that is consistent with the reported reliance of such tissue on glycolysis for metabolism.

The role of superoxide and hydrogen peroxide (commonly referred to as ROS) in tumor promotion and inhibition is not fully understood and is dependent on various factors including tumor cell type and tumor stage. ROS generated in low levels stimulates tumor growth, migration, and metastasis [31–34]. Of the many intracellular sources of ROS, both NADPH oxidase enzymes and mitochondria are considered to be major sources of ROS [5, 35–38]. Both superoxide dismutase and glutathione peroxidase mimics were reported to block tumor proliferation and metastasis in cancer cells and mice xenografts, thus implicating the role of superoxide and H_2O_2 [39]. Many years ago, NADPH oxidase (Nox)-derived H_2O_2 was shown to be responsible for enhanced proliferation of prostate cancer, and reports also suggest that Nox4 supports renal tumorigenesis via enhanced formation of ROS [35]. Nox isoforms have been proposed as potential therapeutic targets in the treatment of cancer and other diseases [40, 41]. Unlike other redox enzymes for which ROS generation is an accidental byproduct of their catalytic function, the only known function of Nox is generation of ROS [42]. Clearly, Nox-derived ROS have been shown to play a significant role in the tumor microenvironment.

Cancer cells constantly reprogram their metabolism by developing adaptive responses to meet increased energetic demands in order to sustain rapid growth and survival [43–45]. Although enhanced aerobic glycolysis is a preferred pathway for cancer cells to acquire metabolic needs (the Warburg effect), it is increasingly evident that many tumors require OXPHOS or mitochondrial respiration for their growth and survival [46–48]. Reports suggest that metabolic reprogramming—from a glycolytic phenotype to OXPHOS—occurs during tumorigenesis or during oncogenic kinase inhibition in cancer cells [49, 50]. Inhibitors of kinase (which often decrease glycolysis) enhance drug resistance accompanied by increased OXPHOS [51]. Enhanced OXPHOS increased mitochondrial ROS formation as has been reported in yeast and mammalian cells [52, 53]. Cancer cells develop adaptive responses to increased ROS through upregulation of antioxidant machinery (*e.g.*, Keap1-Nrf2 pathway) or transcription factor PPAR-γ coactivator-1α (PGC-1α) [54, 55]. Although several reports provide evidence for enhanced ROS formation (using fluorescent dyes) in

Author Manuscript Author Manuscript Author Manuscript Author Manuscript

tumor cells [56, 57], direct evidence for enhanced ROS formation or a ROS-induced oxidative biomarker in tumor tissues has been lacking. Monitoring changes in oxidant formation in an *in vivo* setting following drug resistance and metabolic reprogramming is crucial for developing precise and effective antitumor therapy. The low-temperature EPR technique developed here is ideal for detecting aconitase inactivation as a marker of mitochondrial superoxide produced from mitochondrial electron transport. The oxidized aconitase signal has previously been used as a marker of oxidative stress in biological systems [15]. In addition to detecting the endogenous mitochondrial oxidative stress biomarker protein, aconitase, the EPR technique is also able to measure the oxidation states of redox-active mitochondrial components (iron-sulfur clusters, hemes) in mitochondrial complexes. For the first time, using the EPR technique and histologically distinct inner and outer sections of large tumors, we were able to obtain new information on tumor heterogeneity with respect to mitochondrial redox changes (Fig. 5).

The bioluminescence imaging technique with luciferin as a bioluminescent probe is routinely used to monitor tumor growth in mice xenografts [58, 59]. This approach enables measurement in tumor cells due to selective localization of luciferase in tumor cells. Here, we show that the same detection modality can be used to monitor ROS formation in tumor cells using the luciferin precursor, PCL-1, as an ROS probe.

ROS (*e.g.*, H_2O_2, $ONOO^-$, and HOCl) can oxidize PCL-1 to luciferin and induce bioluminescence in luciferin-transfected tumors [19–21, 30]. We have previously shown that $ONOO^-$ and HOCl react with boronate-based probes such as PCL-1 much more rapidly than H_2O_2 [21]. In order to accurately specify the oxidant responsible for bioluminescence, it is essential to identify the specific minor products (nitrated or chlorinated PCL-1 and/or luciferin) in tumors using the LC/MS technique [21]. Antioxidant enzymes (*e.g.*, PEG-catalase), catalytic peroxide scavengers, and nitric oxide synthase inhibitors may be used to distinguish between various oxidants, but their ability to alter tumor growth may be a confounding factor. ROS/PCL-1 BLI may also have other limitations. For example, although we observed very little bioluminescence in tumor tissues at luciferin levels that might be present in PCL-1 as an impurity, we cannot dismiss the likelihood of extraneous metabolism of PCL-1 outside the tumor (*e.g.*, in the liver) to luciferin. Both luciferin and PCL-1 were reportedly cleared within hours and, to our knowledge, the role of Phase-1 and Phase-2 enzymes in the metabolism of luciferin and PCL-1 has not been determined. Another possibility is oxidation of PCL-1 within the tumor microenvironment to luciferin in the same xenograft model. Although we demonstrate the ability of the PCL-1 probe to detect oxidants in tumor models *in vivo*, further studies on probe pharmacokinetics and identification of the oxidants involved in PCL-1 conversion to luciferin, and other products clearly are necessary.

Glutathione peroxidases (GPx) and peroxiredoxins (Prxs) are major targets for H_2O_2 in cells. Detailed kinetic analyses indicate that Prxs react with H_2O_2 nearly a million times faster than with other redox probes (*e.g.*, PCL-1) [21]. Most boronate-based probes including PCL-1 react with H_2O_2 ($k \simeq 1\ M^{-1}s^{-1}$) much slower than with $ONOO^-$ ($k \simeq 10^6\ M^{-1}s^{-1}$) or HOCl ($k \simeq 10^4\ M^{-1}s^{-1}$) [60]. In the presence of bicarbonate at physiological concentrations (~25 mM), H_2O_2 reactivity with thiols can be increased through the intermediate formation of a hyperoxidizing species, HCO_4^- [61]. It is likely that HCO_4^-/

Author Manuscript Author Manuscript Author Manuscript Author Manuscript

boronate reactivity is enhanced compared to H_2O_2; however, a major limitation of using PCL-1 or other analogous probes for H_2O_2 detection is the slow reactivity of boronate-based probes with H_2O_2 compared to the endogenous H_2O_2 detoxifying enzymes (*e.g.*, GPx and Prxs), limiting the sensitivity of the assay.

Radio-labeled hydroethidine-based fluorescent probes have been used to image ROS in animal models [62, 63]. Recently, a positron emission tomography (PET) tracer, ^{18}F-labeled hydromethidine (^{18}F-DHMT) was used to detect superoxide as an early index of doxorubicin-induced cardiomyopathy in rodents [64]. As we have emphasized in previous publications [62], the chemistry between ROS and isotope-labeled or radio-labeled dyes is the same as that described for ROS reactions with unlabeled dyes. Thus, it is incorrect to conclude that PET imaging arises from the superoxide-derived product (*i.e.*, ^{18}F-2OH-M$^+$) and not from the ^{18}F-labeled other oxidation product, ^{18}F-M$^+$, or to ^{18}F-labeled methidium dimers (^{18}F-M$^+$–^{18}F-M$^+$) [62]. In other studies, using hyperpolarized ^{13}C-thiourea, detection of H_2O_2 in a mouse liver was reported [65]. Thiourea is oxidized by H_2O_2 to thiourea dioxide that is subsequently hydrolyzed to urea [65]. Although the reaction chemistry is established, the second-order rate constant between H_2O_2 and thiourea (k=0.08 $M^{-1}s^{-1}$) is even slower than the reaction between H_2O_2 and boronate-based probes. Thus, molar levels of hyperpolarized ^{13}C-thiourea were intravenously administered for imaging experiments. Clearly, in order to make fluorescent probe or PET-tracer-based imaging of ROS a viable approach in diseased animal models that can be extended into the clinic, the probes should be nontoxic and react stoichiometrically and more rapidly with H_2O_2.

The low-temperature EPR technique developed here can be translated to studies using surgically removed tumor tissues in the clinic. The EPR technique may be the only viable analytical approach that will enable detection of mitochondrial redox status and oxidative biomarkers in clinically isolated human tumors. It is conceivable that one can obtain deeper insight with regard to metabolic reprogramming that can help predict whether these tumors will be susceptible or not to OXPHOS inhibitors. Enhanced expertise in image analyses may make it possible to assess the redox heterogeneity in tumor tissues by monitoring the bioluminescence intensity emitted from the inner and outer sections of the tumor. Several drugs and superoxide dismutase mimetics (Tempol) have been shown to inhibit tumor growth that was attributed to dismutation or detoxification of ROS [34]. The *ex vivo* EPR methodology is suitable for testing this mechanism. Going forward, it will be of interest to extend the *ex vivo* studies to immune competent mice tumor xenografts that can provide additional insights on ROS production from immune cells in the tumor microenvironment in response to immune-modulating treatments.

Supplementary Material

Refer to Web version on PubMed Central for supplementary material.

Acknowledgements

This work was supported by the Medical College of Wisconsin Cancer Center. Low-temperature EPR was supported in part by NSF Major Research Instrumentation award CHE-1532168 to BB and by the National Cancer Institute of the National Institutes of Health under Award Numbers U01 CA178960 and R01 CA208648. R.P. was

Author Manuscript Author Manuscript Author Manuscript Author Manuscript

supported by Polish National Science Centre within the SONATA BIS program (Grant Number 2016/22/E/ST4/00549). The content is solely the responsibility of the authors and does not necessarily represent the official views of the National Institutes of Health.

References

[1]. Gorrini C, Harris IS, Mak TW, Modulation of oxidative stress as an anticancer strategy, Nat Rev Drug Discov 12(12) (2013) 931–47. [PubMed: 24287781]

[2]. Chio IIC, Tuveson DA, ROS in Cancer: The Burning Question, Trends Mol Med 23(5) (2017) 411–429. [PubMed: 28427863]

[3]. Idelchik M, Begley U, Begley TJ, Melendez JA, Mitochondrial ROS control of cancer, Semin Cancer Biol 47 (2017) 57–66. [PubMed: 28445781]

[4]. Weinberg F, Hamanaka R, Wheaton WW, Weinberg S, Joseph J, Lopez M, Kalyanaraman B, Mutlu GM, Budinger GR, Chandel NS, Mitochondrial metabolism and ROS generation are essential for Kras-mediated tumorigenicity, Proceedings of the National Academy of Sciences of the United States of America 107(19) (2010) 8788–93. [PubMed: 20421486]

[5]. Diebold L, Chandel NS, Mitochondrial ROS regulation of proliferating cells, Free Radic Biol Med 100 (2016) 86–93. [PubMed: 27154978]

[6]. Durand N, Storz P, Targeting reactive oxygen species in development and progression of pancreatic cancer, Expert Rev Anticancer Ther 17(1) (2017) 19–31. [PubMed: 27841037]

[7]. Chandel NS, Tuveson DA, The promise and perils of antioxidants for cancer patients, N Engl J Med 371(2) (2014) 177–8. [PubMed: 25006725]

[8]. Wang J, Yi J, Cancer cell killing via ROS: to increase or decrease, that is the question, Cancer Biol Ther 7(12) (2008) 1875–84. [PubMed: 18981733]

[9]. Omenn GS, Goodman GE, Thornquist MD, Balmes J, Cullen MR, Glass A, Keogh JP, Meyskens FL, Valanis B, Williams JH, Barnhart S, Hammar S, Effects of a combination of beta carotene and vitamin A on lung cancer and cardiovascular disease, N Engl J Med 334(18) (1996) 1150–5. [PubMed: 8602180]

[10]. Piskounova E, Agathocleous M, Murphy MM, Hu Z, Huddlestun SE, Zhao Z, Leitch AM, Johnson TM, DeBerardinis RJ, Morrison SJ, Oxidative stress inhibits distant metastasis by human melanoma cells, Nature 527(7577) (2015) 186–91. [PubMed: 26466563]

[11]. Vance TM, Su J, Fontham ET, Koo SI, Chun OK, Dietary antioxidants and prostate cancer: a review, Nutr Cancer 65(6) (2013) 793–801. [PubMed: 23909722]

[12]. Bennett B, Helbling D, Meng H, Jarzembowski J, Geurts AM, Friederich MW, Van Hove JL, Lawlor MW, Dimmock DP, Potentially diagnostic electron paramagnetic resonance spectra elucidate the underlying mechanism of mitochondrial dysfunction in the deoxyguanosine kinase deficient rat model of a genetic mitochondrial DNA depletion syndrome, Free Radical Biol Med 92 (2016) 141–51. [PubMed: 26773591]

[13]. Myers CR, Antholine WE, Myers JM, The pro-oxidant chromium(VI) inhibits mitochondrial complex I, complex II, and aconitase in the bronchial epithelium: EPR markers for Fe-S proteins, Free Radic Biol Med 49(12) (2010) 1903–15. [PubMed: 20883776]

[14]. Kennedy MC, Emptage MH, Dreyer JL, Beinert H, The role of iron in the activation-inactivation of aconitase, J Biol Chem 258(18) (1983) 11098–105. [PubMed: 6309829]

[15]. Cheng G, Zielonka M, Dranka B, Kumar SN, Myers CR, Bennett B, Garces AM, Dias Duarte Machado LG, Thiebaut D, Ouari O, Hardy M, Zielonka J, Kalyanaraman B, Detection of mitochondria-generated reactive oxygen species in cells using multiple probes and methods: Potentials, pitfalls, and the future, J Biol Chem 293(26) (2018) 10363–10380. [PubMed: 29739855]

[16]. Kalyanaraman B, Cheng G, Zielonka J, Bennett B, Low-Temperature EPR Spectroscopy as a Probe-Free Technique for Monitoring Oxidants Formed in Tumor Cells and Tissues: Implications in Drug Resistance and OXPHOS-Targeted Therapies, Cell Biochem Biophys 77(1) (2019) 89–98. [PubMed: 30259334]

[17]. Cheng G, Zielonka J, McAllister DM, Mackinnon AC Jr., Joseph J, Dwinell MB, Kalyanaraman B, Mitochondria-targeted vitamin E analogs inhibit breast cancer cell energy metabolism and promote cell death, BMC Cancer 13 (2013) 285. [PubMed: 23764021]

Author Manuscript Author Manuscript Author Manuscript Author Manuscript

[18]. Cheng G, Zielonka J, Dranka BP, McAllister D, Mackinnon AC Jr., Joseph J, Kalyanaraman B, Mitochondria-targeted drugs synergize with 2-deoxyglucose to trigger breast cancer cell death, Cancer Res 72(10) (2012) 2634–44. [PubMed: 22431711]

[19]. Van De Bittner GC, Dubikovskaya EA, Bertozzi CR, Chang CJ, In vivo imaging of hydrogen peroxide production in a murine tumor model with a chemoselective bioluminescent reporter, Proceedings of the National Academy of Sciences of the United States of America 107(50) (2010) 21316–21321. [PubMed: 21115844]

[20]. Van De Bittner GC, Bertozzi CR, Chang CJ, Strategy for dual-analyte luciferin imaging: In vivo bioluminescence detection of hydrogen peroxide and caspase activity in a murine model of acute inflammation, J Am Chem Soc 135(5) (2013) 1783–1795. [PubMed: 23347279]

[21]. Zielonka J, Podsiadly R, Zielonka M, Hardy M, Kalyanaraman B, On the use of peroxy-caged luciferin (PCL-1) probe for bioluminescent detection of inflammatory oxidants in vitro and in vivo - Identification of reaction intermediates and oxidant-specific minor products, Free Radical Biol Med 99 (2016) 32–42. [PubMed: 27458121]

[22]. Johnson MK, Thomson AJ, Richards AJ, Peterson J, Robinson AE, Ramsay RR, Singer TP, Characterization of the Fe-S cluster in aconitase using low temperature magnetic circular dichroism spectroscopy, J Biol Chem 259(4) (1984) 2274–82. [PubMed: 6698964]

[23]. Kennedy MC, Antholine WE, Beinert H, An EPR investigation of the products of the reaction of cytosolic and mitochondrial aconitases with nitric oxide, J Biol Chem 272(33) (1997) 20340–7. [PubMed: 9252338]

[24]. Langley M, Ghosh A, Charli A, Sarkar S, Ay M, Luo J, Zielonka J, Brenza T, Bennett B, Jin H, Ghaisas S, Schlichtmann B, Kim D, Anantharam V, Kanthasamy A, Narasimhan B, Kalyanaraman B, Kanthasamy AG, Mito-Apocynin Prevents Mitochondrial Dysfunction, Microglial Activation, Oxidative Damage, and Progressive Neurodegeneration in MitoPark Transgenic Mice, Antioxid Redox Signal 27(14) (2017) 1048–1066. [PubMed: 28375739]

[25]. Nakajima EC, Laymon C, Oborski M, Hou W, Wang L, Grandis JR, Ferris RL, Mountz JM, Van Houten B, Quantifying metabolic heterogeneity in head and neck tumors in real time: 2-DG uptake is highest in hypoxic tumor regions, PLoS One 9(8) (2014) e102452. [PubMed: 25127378]

[26]. Bomba M, Camagna A, Cannistraro S, Indovina PL, Samoggia P, EPR study of serum ceruloplasmin and iron transferrin in myocardial infarction, Physiol Chem Phys 9(2) (1977) 175–80. [PubMed: 202979]

[27]. Harris DC, Different metal-binding properties of the two sites of human transferrin, Biochemistry 16(3) (1977) 560–4. [PubMed: 189804]

[28]. Dunne J, Caron A, Menu P, Alayash AI, Buehler PW, Wilson MT, Silaghi-Dumitrescu R, Faivre B, Cooper CE, Ascorbate removes key precursors to oxidative damage by cell-free haemoglobin in vitro and in vivo, Biochem J 399(3) (2006) 513–24. [PubMed: 16848758]

[29]. Yang L, Fan M, Du F, Gong Q, Bi ZG, Zhu ZJ, Zhu LL, Ke Y, Hypoxic preconditioning increases iron transport rate in astrocytes, Biochim Biophys Acta 1822(4) (2012) 500–8. [PubMed: 22198321]

[30]. Sieracki NA, Gantner BN, Mao M, Horner JH, Ye RD, Malik AB, Newcomb ME, Bonini MG, Bioluminescent detection of peroxynitrite with a boronic acid-caged luciferin, Free Radic Biol Med 61 (2013) 40–50. [PubMed: 23474271]

[31]. Sullivan LB, Chandel NS, Mitochondrial reactive oxygen species and cancer, Cancer Metab 2 (2014) 17. [PubMed: 25671107]

[32]. Schumacker PT, Reactive oxygen species in cancer: a dance with the devil, Cancer Cell 27(2) (2015) 156–7. [PubMed: 25670075]

[33]. Reczek CR, Chandel NS, ROS Promotes Cancer Cell Survival through Calcium Signaling, Cancer Cell 33(6) (2018) 949–951. [PubMed: 29894695]

[34]. Du J, Nelson ES, Simons AL, Olney KE, Moser JC, Schrock HE, Wagner BA, Buettner GR, Smith BJ, Teoh ML, Tsao MS, Cullen JJ, Regulation of pancreatic cancer growth by superoxide, Mol Carcinog 52(7) (2013) 555–67. [PubMed: 22392697]

Author Manuscript Author Manuscript Author Manuscript Author Manuscript

[35]. Gregg JL, Turner RM 2nd, Chang G, Joshi D, Zhan Y, Chen L, Maranchie JK, NADPH oxidase NOX4 supports renal tumorigenesis by promoting the expression and nuclear accumulation of HIF2alpha, Cancer Res 74(13) (2014) 3501–3511. [PubMed: 24755467]

[36]. Brand MD, Mitochondrial generation of superoxide and hydrogen peroxide as the source of mitochondrial redox signaling, Free Radic Biol Med 100 (2016) 14–31. [PubMed: 27085844]

[37]. Boveris A, Chance B, The mitochondrial generation of hydrogen peroxide. General properties and effect of hyperbaric oxygen, Biochem J 134(3) (1973) 707–16. [PubMed: 4749271]

[38]. Boveris A, Oshino N, Chance B, The cellular production of hydrogen peroxide, Biochem J 128(3) (1972) 617–30. [PubMed: 4404507]

[39]. Alsner J, Yilmaz M, Guldberg P, Hansen LL, Overgaard J, Heterogeneity in the clinical phenotype of TP53 mutations in breast cancer patients, Clin Cancer Res 6(10) (2000) 3923–31. [PubMed: 11051239]

[40]. Weyemi U, Redon CE, Parekh PR, Dupuy C, Bonner WM, NADPH Oxidases NOXs and DUOXs as putative targets for cancer therapy, Anticancer Agents Med Chem 13(3) (2013) 502–14. [PubMed: 22931418]

[41]. Barua S, Kim JY, Yenari MA, Lee JE, The role of NOX inhibitors in neurodegenerative diseases, IBRO Rep 7 (2019) 59–69. [PubMed: 31463415]

[42]. Lambeth JD, NOX enzymes and the biology of reactive oxygen, Nat Rev Immunol 4(3) (2004) 181–9. [PubMed: 15039755]

[43]. DeBerardinis RJ, Lum JJ, Hatzivassiliou G, Thompson CB, The biology of cancer: metabolic reprogramming fuels cell growth and proliferation, Cell Metab 7(1) (2008) 11–20. [PubMed: 18177721]

[44]. Ward PS, Thompson CB, Metabolic reprogramming: a cancer hallmark even warburg did not anticipate, Cancer Cell 21(3) (2012) 297–308. [PubMed: 22439925]

[45]. Vander Heiden MG, Cantley LC, Thompson CB, Understanding the Warburg effect: the metabolic requirements of cell proliferation, Science 324(5930) (2009) 1029–33. [PubMed: 19460998]

[46]. Kalyanaraman B, Cheng G, Hardy M, Ouari O, Bennett B, Zielonka J, Teaching the basics of reactive oxygen species and their relevance to cancer biology: Mitochondrial reactive oxygen species detection, redox signaling, and targeted therapies, Redox Biology 15 (2018) 347–362. [PubMed: 29306792]

[47]. Mullen AR, Wheaton WW, Jin ES, Chen PH, Sullivan LB, Cheng T, Yang Y, Linehan WM, Chandel NS, DeBerardinis RJ, Reductive carboxylation supports growth in tumour cells with defective mitochondria, Nature 481(7381) (2011) 385–8. [PubMed: 22101431]

[48]. Martinez-Reyes I, Diebold LP, Kong H, Schieber M, Huang H, Hensley CT, Mehta MM, Wang T, Santos JH, Woychik R, Dufour E, Spelbrink JN, Weinberg SE, Zhao Y, DeBerardinis RJ, Chandel NS, TCA Cycle and Mitochondrial Membrane Potential Are Necessary for Diverse Biological Functions, Mol Cell 61(2) (2016) 199–209. [PubMed: 26725009]

[49]. Feichtinger RG, Lang R, Geilberger R, Rathje F, Mayr JA, Sperl W, Bauer JW, Hauser-Kronberger C, Kofler B, Emberger M, Melanoma tumors exhibit a variable but distinct metabolic signature, Exp Dermatol 27(2) (2018) 204–207. [PubMed: 29131438]

[50]. De Rosa V, Iommelli F, Monti M, Fonti R, Votta G, Stoppelli MP, Del Vecchio S, Reversal of Warburg Effect and Reactivation of Oxidative Phosphorylation by Differential Inhibition of EGFR Signaling Pathways in Non-Small Cell Lung Cancer, Clin Cancer Res 21(22) (2015) 5110–20. [PubMed: 26216352]

[51]. Gopal YNV, Rizos H, Chen G, Deng W, Frederick DT, Cooper ZA, Scolyer RA, Pupo G, Komurov K, Sehgal V, Zhang J, Patel L, Pereira CG, Broom BM, Mills GB, Ram P, Smith PD, Wargo JA, Long GV, Davies MA, Inhibition of mTORC1/2 overcomes resistance to MAPK pathway inhibitors mediated by PGC1α and Oxidative Phosphorylation in melanoma, Cancer Res 74(23) (2014) 7037–47. [PubMed: 25297634]

[52]. Bouchez C, Devin A, Mitochondrial Biogenesis and Mitochondrial Reactive Oxygen Species (ROS): A Complex Relationship Regulated by the cAMP/PKA Signaling Pathway, Cells 8(4) (2019).

Author Manuscript Author Manuscript Author Manuscript Author Manuscript

[53]. Solaini G, Sgarbi G, Baracca A, Oxidative phosphorylation in cancer cells, Biochim Biophys Acta 1807(6) (2011) 534–42. [PubMed: 20849810]

[54]. Sun X, Wang S, Gai J, Guan J, Li J, Li Y, Zhao J, Zhao C, Fu L, Li Q, SIRT5 Promotes Cisplatin Resistance in Ovarian Cancer by Suppressing DNA Damage in a ROS-Dependent Manner via Regulation of the Nrf2/HO-1 Pathway, Front Oncol 9 (2019) 754. [PubMed: 31456942]

[55]. Bruns I, Sauer B, Burger MC, Eriksson J, Hofmann U, Braun Y, Harter PN, Luger AL, Ronellenfitsch MW, Steinbach JP, Rieger J, Disruption of peroxisome proliferator-activated receptor gamma coactivator (PGC)-1alpha reverts key features of the neoplastic phenotype of glioma cells, J Biol Chem 294(9) (2019) 3037–3050. [PubMed: 30578297]

[56]. Figueroa D, Asaduzzaman M, Young F, Real time monitoring and quantification of reactive oxygen species in breast cancer cell line MCF-7 by 2',7'-dichlorofluorescin diacetate (DCFDA) assay, J Pharmacol Toxicol Methods 94(Pt 1) (2018) 26–33. [PubMed: 29630935]

[57]. Kunoh T, Shimura T, Kasai T, Matsumoto S, Mahmud H, Khayrani AC, Seno M, Kunoh H, Takada J, Use of DNA-generated gold nanoparticles to radiosensitize and eradicate radioresistant glioma stem cells, Nanotechnology 30(5) (2019) 055101. [PubMed: 30499457]

[58]. Carroll RG, Zaslona Z, Galvan-Pena S, Koppe EL, Sevin DC, Angiari S, Triantafilou M, Triantafilou K, Modis LK, O'Neill LA, An unexpected link between fatty acid synthase and cholesterol synthesis in proinflammatory macrophage activation, J Biol Chem 293(15) (2018) 5509–5521. [PubMed: 29463677]

[59]. Cheng G, Zielonka J, Ouari O, Lopez M, McAllister D, Boyle K, Barrios CS, Weber JJ, Johnson BD, Hardy M, Dwinell MB, Kalyanaraman B, Mitochondria-Targeted Analogues of Metformin Exhibit Enhanced Antiproliferative and Radiosensitizing Effects in Pancreatic Cancer Cells, Cancer Res 76(13) (2016) 3904–15. [PubMed: 27216187]

[60]. Sikora A, Zielonka J, Lopez M, Joseph J, Kalyanaraman B, Direct oxidation of boronates by peroxynitrite: mechanism and implications in fluorescence imaging of peroxynitrite, Free Radical Biol Med 47(10) (2009) 1401–7. [PubMed: 19686842]

[61]. Truzzi DR, Coelho FR, Paviani V, Alves SV, Netto LES, Augusto O, The bicarbonate/carbon dioxide pair increases hydrogen peroxide-mediated hyperoxidation of human peroxiredoxin 1, J Biol Chem 294(38) (2019) 14055–14067. [PubMed: 31366734]

[62]. Kalyanaraman B, Hardy M, Zielonka J, A Critical Review of Methodologies to Detect Reactive Oxygen and Nitrogen Species Stimulated by NADPH Oxidase Enzymes: Implications in Pesticide Toxicity, Curr Pharmacol Rep 2(4) (2016) 193–201. [PubMed: 27774407]

[63]. Wilson AA, Sadovski O, Nobrega JN, Raymond RJ, Bambico FR, Nashed MG, Garcia A, Bloomfield PM, Houle S, Mizrahi R, Tong J, Evaluation of a novel radiotracer for positron emission tomography imaging of reactive oxygen species in the central nervous system, Nucl Med Biol 53 (2017) 14–20. [PubMed: 28719807]

[64]. Boutagy NE, Wu J, Cai Z, Zhang W, Booth CJ, Kyriakides TC, Pfau D, Mulnix T, Liu Z, Miller EJ, Young LH, Carson RE, Huang Y, Liu C, Sinusas AJ, In Vivo Reactive Oxygen Species Detection With a Novel Positron Emission Tomography Tracer, (18)F-DHMT, Allows for Early Detection of Anthracycline-Induced Cardiotoxicity in Rodents, JACC Basic Transl Sci 3(3) (2018) 378–390. [PubMed: 30062224]

[65]. Wibowo A, Park JM, Liu SC, Khosla C, Spielman DM, Real-Time in Vivo Detection of H2O2 Using Hyperpolarized (13)C-Thiourea, ACS Chem Biol 12(7) (2017) 1737–1742. [PubMed: 28452454]

Author Manuscript Author Manuscript Author Manuscript Author Manuscript

Highlights

- ROS formation is enhanced during tumor growth
- Ex vivo EPR is suitable for detecting oxidative biomarker and iron-sulfur centers
- In vivo bioluminescence monitors tumor size, oxidants, and ATP in mice xenografts

Author Manuscript Author Manuscript Author Manuscript Author Manuscript

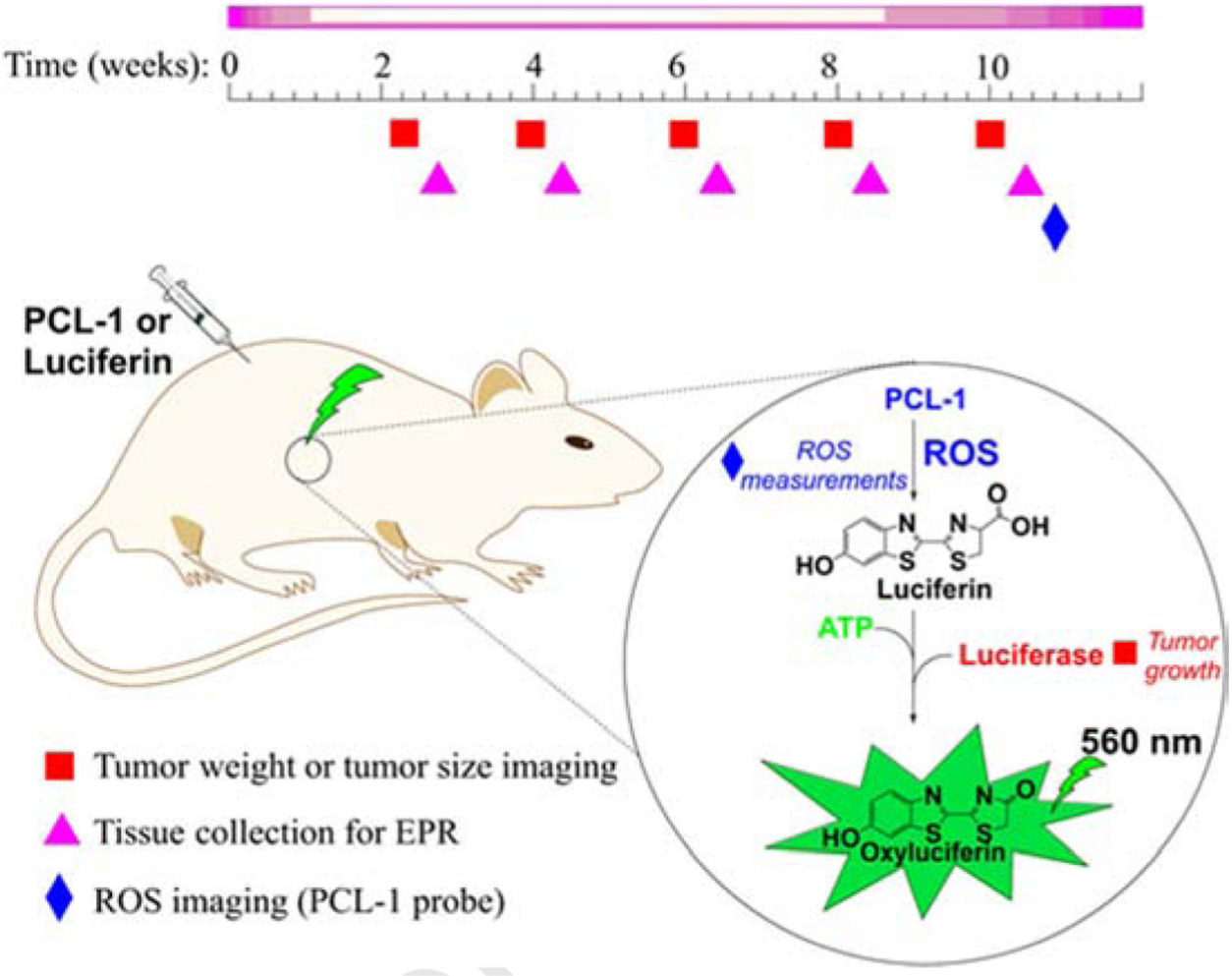

Figure 1.

The experimental design for *ex vivo* EPR and *in vivo* bioluminescence studies monitoring ROS and tumor growth in an MDA-MB-231-luc transfected mouse xenograft model.

Author Manuscript Author Manuscript Author Manuscript Author Manuscript

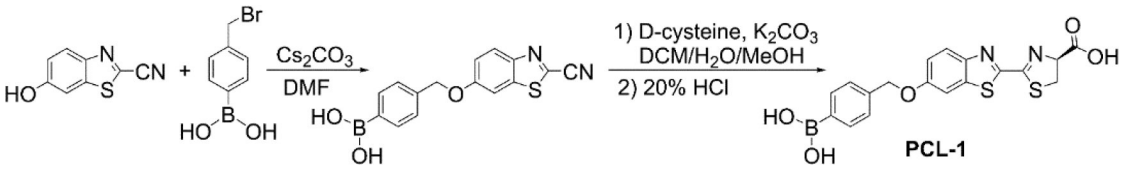

Figure 2.
Synthetic pathway for preparation of the PCL-1 probe.

Author Manuscript Author Manuscript Author Manuscript Author Manuscript

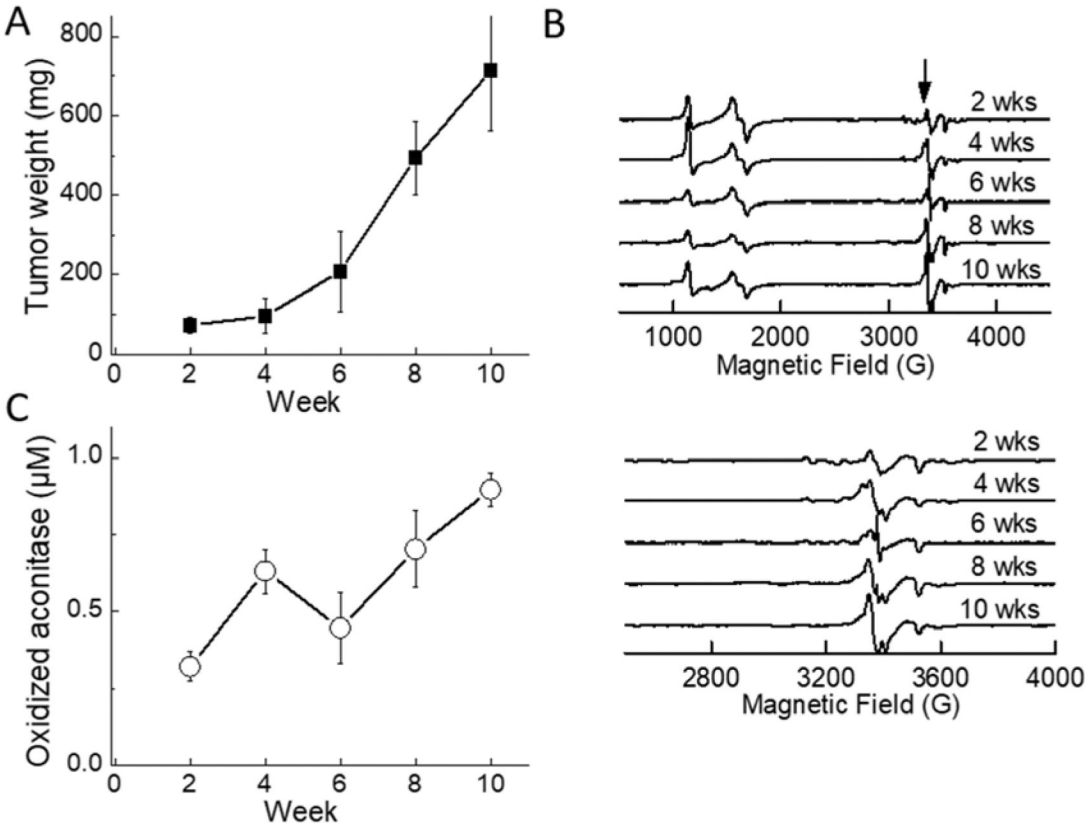

Figure 3.

Ex vivo measurements of tumor tissues isolated from an MDA-MB-231-luc mouse xenograft model. **(A)** Tumor weight as a function of time after implantation. **(B)** EPR spectra of tumor tissues as a function of time (top). The arrow indicates the line position of the oxidized aconitase $[3Fe4S]^{+}$ signal and (bottom) same as above but using an expanded scale. **(C)** Quantification of oxidized aconitase signal as a function of tumor growth. The EPR spectra shown are averaged spectra from either six mice (2 weeks), or three mice (4–10 weeks). In the case of 2-week mice, tumors from two mice were used to provide each EPR sample, *i.e.*, spectra were averaged from three samples total. For 4- and 6-week mice, one tumor from each mouse provided one sample and spectra were averaged from the three samples in each case. For 8-and 10-week mice, one tumor provided two samples, so six spectra were averaged in each case.

Author Manuscript Author Manuscript Author Manuscript Author Manuscript

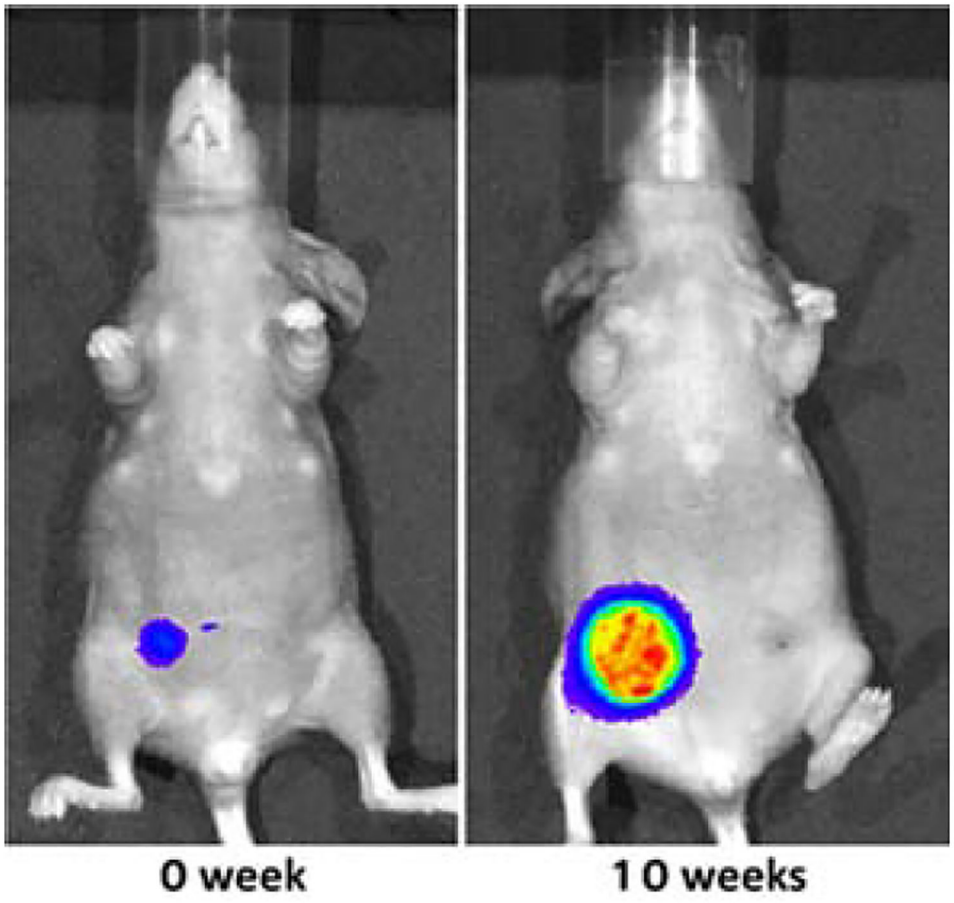

Figure 4.
Bioluminescence-based monitoring of the tumor growth in an MDA-MB-231-luc-based mouse xenograft model.

Author Manuscript Author Manuscript Author Manuscript Author Manuscript

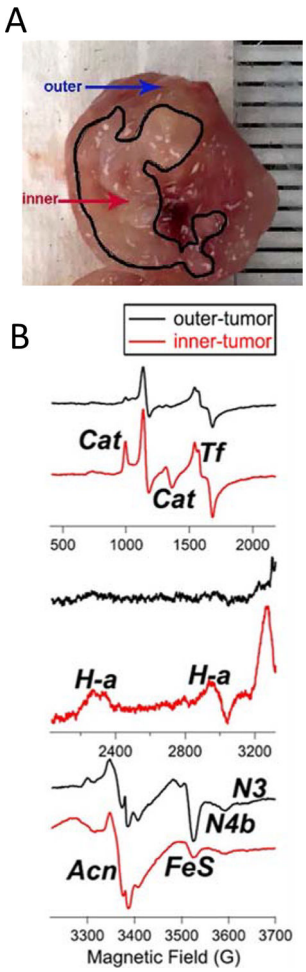

Figure 5. ***Ex vivo*** **EPR showing tumor heterogeneity.**

(A) Breast cancer tumor isolated from breast cancer mice xenografts, 10 weeks after implantation of MDA-MB-231-luc cells. The inner and outer core are marked. **(B)** EPR signals from outer and inner tumor tissues. The EPR spectra (*top, middle, bottom*) show signals obtained over a range of magnetic fields (500–3700 G). The signals are labeled as follows: *Cat*, ferriheme in catalase; *Tf*, Fe(III) in transferrin; *H-a*, heme *a* from Complex IV; *N3* and *N4b*, g_3 resonances from the low-potential N3 and N4 iron-sulfur clusters of Complex I; *Acn*, aconitase $[3Fe4S]^+$; and *FeS*, a composite signal due to g_2 or $g\perp$ resonances from Complex I (N1b, N2, N3, N4) and Complex II (S1, S2) reduced $[2Fe2S]^+$ and $[4Fe4S]^+$ signals.

Author Manuscript Author Manuscript Author Manuscript Author Manuscript

Figure 6.

Chemical basis for PCL-1-based *in vivo* bioluminescent monitoring of reactive oxygen and reactive nitrogen species.

Author Manuscript Author Manuscript Author Manuscript Author Manuscript

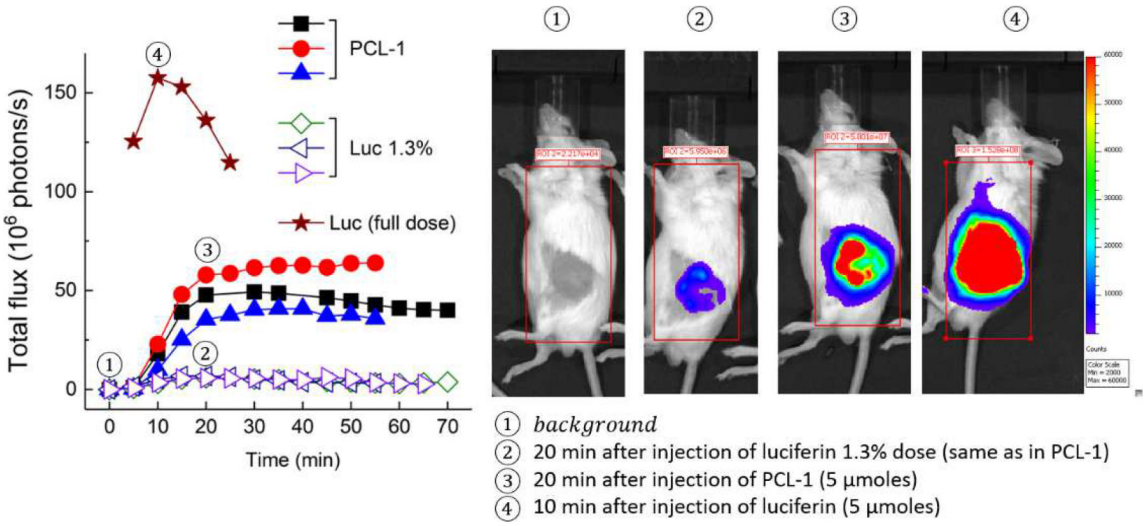

Figure 7.

(Left) Comparison of the dynamics of bioluminescence increase and decay from luciferin and PCL-1 (each 5 μmoles) in an MDA-MB-231-luc-based mouse xenograft model (10 weeks after tumor implantation). Luciferin (1.3%) represents the amount of luciferin impurity in the PCL-1 probe preparation. **(Right)** PCL-1- and Luc-derived bioluminescence imaging in mice xenografts at time points (1–4) indicated on the graph (left).

Author Manuscript Author Manuscript Author Manuscript Author Manuscript

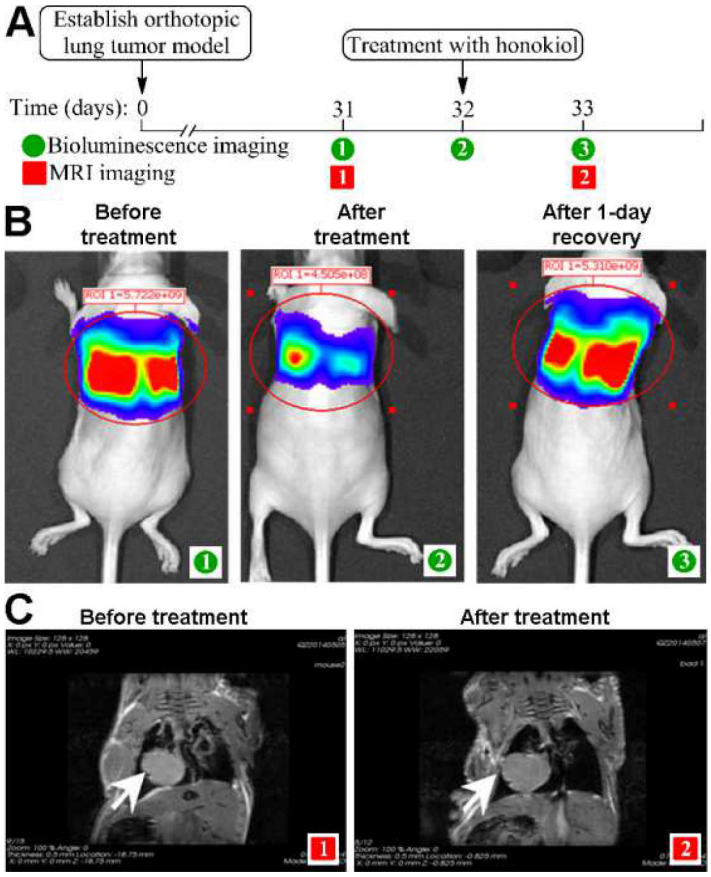

Figure 8.

In vivo monitoring of tumor tissue ATP level after honokiol injection using BLI. **(A)** Experimental protocol. **(B–C)** Images of mice before and after honokiol treatment using bioluminescence **(B)** and MRI **(C)** modalities.